In this case we have a unique isolated minimum. Let there be a singular point at the origin such that $E(0,0) = 0$. We conclude that $(p,q) = (0,0)$ at this point. If the surface is smooth enough, we can expand z as a power series in x and y with the first-order terms missing. If we also ignore higher-order terms near the origin, we can write

$$z = z_0 + \frac{1}{2}(ax^2 + 2bxy + cy^2).$$

Thus

$$p = ax + by \qquad \text{and} \qquad q = bx + cy.$$

Substituting these values in the formula for the reflectance map, we obtain

$$E(x,y) = \frac{1}{2}(a^2 + b^2)x^2 + (a+c)bxy + \frac{1}{2}(b^2 + c^2)y^2.$$

Our task is to determine the coefficients a, b, and c, given the image brightness and its derivatives near the origin. Before we go on, observe that the surface

$$z = z_0 - \frac{1}{2}\left(ax^2 + bxy + \frac{1}{2}cy^2\right)$$

gives rise to exactly the same shading pattern, so we already know that there will be at least two solutions.

The brightness gradient is given by

$$E_x = (a^2 + b^2)x + (a+c)b\,y,$$

$$E_y = (a+c)b\,x + (b^2 + c^2)y.$$

Thus $(E_x, E_y)^T = (0,0)^T$ at $(x,y) = (0,0)$, as it should. We cannot use the brightness gradient to recover the shape. Differentiating again, we obtain the three equations

$$E_{xx} = a^2 + b^2, \quad E_{xy} = (a+c)b, \quad E_{yy} = b^2 + c^2,$$

in the three unknowns a, b, and c. Three second-order polynomials in three unknowns can have up to eight solutions. The three equations found here have a rather special form, however, and there are only four solutions, as shown in exercise 11-10.

In any case, given one of these local solutions, we can construct a small cap. The edge of this region then constitutes an initial strip for the method of characteristic strip expansion, since p and q as well as z are known on the edge. Note also that the solution will move away from the edge, since R_p and R_q are nonzero there.

The above analysis can be generalized to singular points away from the origin and to other rotationally symmetric reflectance maps. It provides a means for starting a solution a small distance away from the singular point. A possible problem is that more than one shape might give rise to the same shading, since the nonlinear equations containing the coefficients of the power series near the singular point can have more than one solution, as they did here.

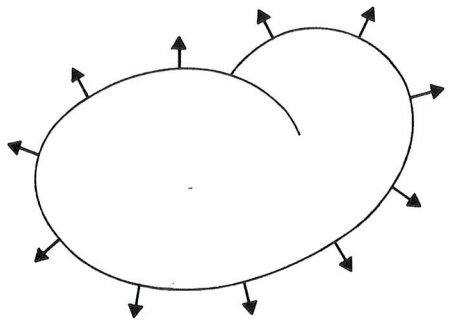

Figure 11-8. The occluding boundary provides an important constraint on the solutions of the shape-from-shading problem. The surface orientation of any solution has to match the known surface orientation along the silhouette.

11.5 Occluding Boundaries

At what other point is the surface orientation known? If the object has a smooth surface, then the silhouette also provides valuable information (figure 11-8). The occluding boundary is the curve on the surface that projects to the silhouette. The orientation there is known, since the tangent plane includes the direction to the observer and also the tangent at the corresponding point on the silhouette. In other words, the surface normal on the occluding boundary lies in a plane parallel to the image plane and is perpendicular to the silhouette.

The only problem with this kind of information is that the slope of the surface is infinite on the occluding boundary. It is thus difficult to incorporate this information as an "initial curve." Nevertheless, it is possible to show that if the reflectance map is a strictly monotonic function of a quadratic function of p and q, then there is a unique surface corresponding to a particular shaded image that exhibits a simple closed silhouette. Conversely, if the reflectance map is a linear function in p and q, then an infinite number of surfaces gives rise to the same shading. In many cases shading and auxiliary information determine a surface uniquely. In some cases they do not, unfortunately: The shading on a small patch of the

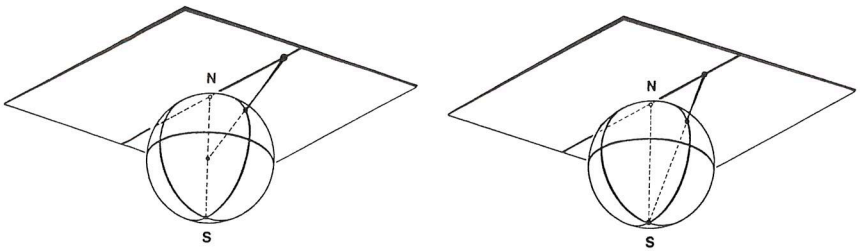

(a) (b)

Figure 11-9. Because points on the Gaussian sphere specify directions in space, the reflectance map can be plotted on the Gaussian sphere. (a) More commonly, we project the upper hemisphere onto an infinite plane, called the gradient space. If we want to deal with the occluding boundary of an object, another projection is more useful. (b) Here, the whole sphere, except for one point, is projected onto a plane, called the stereographic plane. (Figures reproduced with permission from the chapter by Woodham in *Image Understanding 1984*, edited by S. Ullman & W. Richards, Ablex Publishing Corp., Norwood, New Jersey, 1984.)

surface of an object, for example, without any other information, does not determine the local shape of the surface.

11.6 Stereographic Projection

Orientation has two degrees of freedom. We can specify the orientation of a patch by giving its gradient (p, q). Alternatively we can erect a unit normal $\hat{\mathbf{n}}$. As noted in the previous chapter, we can use the Gaussian sphere to represent the direction in which the surface normal is pointing. The Gaussian sphere itself is often inconvenient to use because of its curved surface. This is why we usually project it onto a plane to obtain the *gradient space* (figure 11-9a).

Consider an axis through the sphere parallel to the z-axis. We can project points on the "northern" hemisphere onto a plane tangent at the "north" pole, using the center of the sphere as the center of projection. This is called the *gnomonic* projection. It is easy to show that position in this plane equals $(-p, -q)$. One disadvantage of gradient space (the plane so defined) is that we can only project one hemisphere onto the plane if we want to avoid ambiguity.

Often we are only concerned with surface elements facing the viewer. These correspond to points on the northern hemisphere. But at times directions in the other hemisphere are needed also. In a scene lit from behind, for example, the direction to the light source can be specified by a point in the southern hemisphere. We just came across another difficulty with

gradient space. Orientations of surface patches on the occluding boundary correspond to points on the equator of the Gaussian sphere, which project to infinity in gradient space.

One way out of these difficulties is provided by the *stereographic projection.* Here again we project onto a plane tangent at the north pole, but this time the center of projection is the south pole (figure 11-9b). All points on the sphere, except for the south pole, can be mapped. The equator projects to a circle of radius two. Let us call the coordinates in stereographic space f and g. We show in exercise 11-13 that

$$f = \frac{2p}{1+\sqrt{1+p^2+q^2}} \quad \text{and} \quad g = \frac{2q}{1+\sqrt{1+p^2+q^2}}.$$

Conversely,

$$p = \frac{4f}{4-f^2-g^2} \quad \text{and} \quad q = \frac{4g}{4-f^2-g^2}.$$

An added advantage of stereographic space is that it is a conformal projection of the Gaussian sphere. That is, angles on the surface of the sphere are projected faithfully into equal angles in the plane. One disadvantage, however, is that some formulae become more complicated when expressed in stereographic coordinates.

11.7 Relaxation Methods

The method of characteristic strip expansion suffers from a number of practical problems, including sensitivity to measurement noise. Special means must be employed to prevent adjacent characteristics from crossing over each other as a result of small errors accumulating in the numerical integration of the differential equations. This method also makes it hard to utilize the information on surface orientation available on the occluding boundary. Finally, it suggests neither biological nor parallel machine implementations.

More desirable would be an iterative scheme similar to one of the finite-difference methods used for solving elliptic second-order partial differential equations. This would immediately suggest ways to incorporate boundary and other auxiliary information.

11.7.1 Minimization in the Continuous Case

Our objective is to find two functions, $f(x, y)$ and $g(x, y)$, that ensure that the image irradiance equation,

$$E(x, y) = R_s(f, g),$$

is satisfied, where $R_s(f,g)$ is the reflectance map expressed in stereographic coordinates. We also want $f(x,y)$ and $g(x,y)$ to correspond to a smooth surface. Of the many ways to measure smoothness, we choose one that penalizes rapid changes in f and g. We try to minimize the integral

$$e_s = \iint_I \left((f_x^2 + f_y^2) + (g_x^2 + g_y^2)\right) dx\, dy,$$

where f_x, f_y, g_x, and g_y are the first partial derivatives of f and g with respect to x and y. Other measures of departure from "smoothness" could also be used. These would lead to somewhat different algorithms.

So far, the plan is to minimize e_s subject to the constraint that f and g must satisfy the image irradiance equation. In practice, there are errors in both the measurements of the irradiance and the determination of the reflectance map. Instead of insisting on equality of $E(x,y)$ and $R_s(f,g)$, we could try to minimize the error

$$e_i = \iint_I \left(E(x,y) - R_s(f,g)\right)^2 dx\, dy.$$

Overall, then, we are to minimize $e_s + \lambda e_i$, where λ is a parameter that weights the errors in the image irradiance equation relative to the departure from smoothness. This parameter should be made large if brightness measurements are very accurate, and small if they are very noisy.

The minimization of an integral of the form

$$\iint F(f, g, f_x, f_y, g_x, g_y)\, dx\, dy$$

is a problem in the calculus of variations (a topic covered in the appendix). The corresponding Euler equations are

$$F_f - \frac{\partial}{\partial x} F_{f_x} - \frac{\partial}{\partial y} F_{f_y} = 0,$$

$$F_g - \frac{\partial}{\partial x} F_{g_x} - \frac{\partial}{\partial y} F_{g_y} = 0,$$

where F_f is the partial derivative of F with respect to f. In the present case,

$$F = (f_x^2 + f_y^2) + (g_x^2 + g_y^2) + \lambda\left(E(x,y) - R_s(f,g)\right)^2.$$

The aim is to minimize the integral of F. The Euler equations for this problem yield

$$\nabla^2 f = -\lambda\left(E(x,y) - R_s(f,g)\right)\frac{\partial R_s}{\partial f},$$

$$\nabla^2 g = -\lambda\left(E(x,y) - R_s(f,g)\right)\frac{\partial R_s}{\partial g},$$

where

$$\nabla^2 = \frac{\partial^2}{\partial x^2} + \frac{\partial^2}{\partial y^2}$$

is the Laplacian operator. The result is a coupled pair of elliptic second-order partial differential equations. These can be solved by iterative methods once the values of f and g on the silhouette are introduced.

11.7.2 Minimization in the Discrete Case

We can develop a numerical method either by approximating the continuous solution found in the previous section or by directly minimizing a discrete version of the integral. Readers uncomfortable with the calculus of variations may be more satisfied with the latter approach. We can measure the departure from smoothness at the point (i,j) by

$$s_{i,j} = \frac{1}{4}\big((f_{i+1,j} - f_{i,j})^2 + (f_{i,j+1} - f_{i,j})^2 + (g_{i+1,j} - g_{i,j})^2 + (g_{i,j+1} - g_{i,j})^2\big),$$

while the error in the image irradiance equation is given by

$$r_{ij} = \left(E_{ij} - R_s(f_{ij}, g_{ij})\right)^2,$$

where E_{ij} is the observed image irradiance at the grid point (i,j). We seek a set of values $\{f_{ij}\}$ and $\{g_{ij}\}$ that minimize

$$e = \sum_i \sum_j (s_{ij} + \lambda r_{ij}).$$

Differentiating e with respect to f_{kl} and g_{kl}, we obtain

$$\frac{\partial e}{\partial f_{kl}} = 2(f_{kl} - \overline{f}_{kl}) - 2\lambda\left(E_{kl} - R_s(f_{kl}, g_{kl})\right)\frac{\partial R_s}{\partial f},$$

$$\frac{\partial e}{\partial g_{kl}} = 2(g_{kl} - \overline{g}_{kl}) - 2\lambda\left(E_{kl} - R_s(f_{kl}, g_{kl})\right)\frac{\partial R_s}{\partial g},$$

where $\overline{f}$ and $\overline{g}$ are local averages of f and g:

$$\overline{f}_{i,j} = \frac{1}{4}\left(f_{i+1,j} + f_{i,j+1} + f_{i-1,j} + f_{i,j-1}\right),$$

$$\overline{g}_{i,j} = \frac{1}{4}\left(g_{i+1,j} + g_{i,j+1} + g_{i-1,j} + g_{i,j-1}\right).$$

We have to be careful when performing this differentiation, since f_{kl} and g_{kl} occur in four terms of the sum; the new subscripts k and l are introduced to avoid confusion with the subscripts i and j that occur in the sum.

The extremum is to be found where the above derivatives of e are equal to zero. If we rearrange the resulting equations by solving for f_{kl} and g_{kl}, an iterative solution method suggests itself:

$$f_{kl}^{n+1} = \overline{f}_{kl}^{n} + \lambda\big(E_{kl} - R_s(f_{kl}^n, g_{kl}^n)\big)\frac{\partial R_s}{\partial f},$$

$$g_{kl}^{n+1} = \overline{g}_{kl}^{n} + \lambda\big(E_{kl} - R_s(f_{kl}^n, g_{kl}^n)\big)\frac{\partial R_s}{\partial g},$$

where the new values for f and g at each grid point are obtained using the old values of f and g in evaluating $R_s(f,g)$, $\partial R_s/\partial f$, and $\partial R_s/\partial g$. It can be shown that a stable method is obtained if we use the local averages $\overline{f}$ and $\overline{g}$ in evaluating $R_s(f,g)$ and the two partial derivatives, provided suitable boundary conditions are introduced and λ is small enough.

The simple iterative scheme described above can be improved in various ways. The estimates of the Laplacians of f and g, proportional to $(\overline{f}_{kl} - f_{kl})$ and $(\overline{g}_{kl} - g_{kl})$, can be replaced by more accurate formulae, for example. Then the local average is computed as

$$\overline{f}_{i,j} = \frac{1}{5}(f_{i+1,j} + f_{i,j+1} + f_{i-1,j} + f_{i,j-1}) + \frac{1}{20}(f_{i+1,j+1} + f_{i+1,j-1} + f_{i-1,j-1} + f_{i-1,j+1}),$$

and similarly for $\overline{g}_{i,j}$. The computation of the average can be represented by the stencil

$$\frac{1}{20}\begin{array}{|c|c|c|}\hline 1 & 4 & 1 \\ \hline 4 & & 4 \\ \hline 1 & 4 & 1 \\ \hline\end{array}$$

which is derived directly from one we used earlier to approximate the Laplacian operator.

Figure 11-10 shows a picture made from the image of a small resin droplet obtained by means of a scanning electron microscope. To apply the iterative shape-from-shading scheme, we have to know the reflectance map. A commonly used model of secondary electron emission from a surface suggests that brightness should vary as the secant of the incident angle, $\sec\theta_i$. Using this model, we obtained the shape shown in figure 11-11.

11.7.3 Application to Photometric Stereo

The gradient values computed at adjacent image points using the photometric stereo method are not necessarily consistent. Even in the case of a planar surface, there can be fluctuations in estimated surface orientation due to measurement errors. If we know that the surface is smooth, we can use the method presented in this chapter to improve the results of the photometric stereo method.

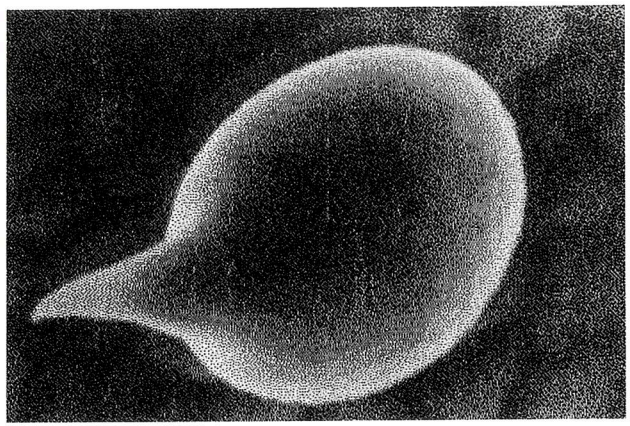

Figure 11-10. Display of the image of a small resin droplet on a flower of a *Cannabis sativa* plant. (Reproduced by permission from the book *Magnifications—Photography with the Scanning Electron Microscope* by David Scharf, Schocken Books, New York, 1977.)

If there are n images, we can formulate this problem in terms of the minimization of

$$e = \iint_I \left((f_x^2 + f_y^2) + (g_x^2 + g_y^2)\right)\,dx\,dy + \sum_{i=1}^{n} \lambda_i \iint_I (E_i(x,y) - R_i(f,g))^2\,dx\,dy,$$

where E_i is the brightness measured in the i^{th} image and R_i is the corresponding reflectance map. The constant multipliers λ_i are parameters that weight the errors in the image irradiance equations relative to the departure from smoothness. They are unequal if the information provided by the cameras is not all equally reliable.

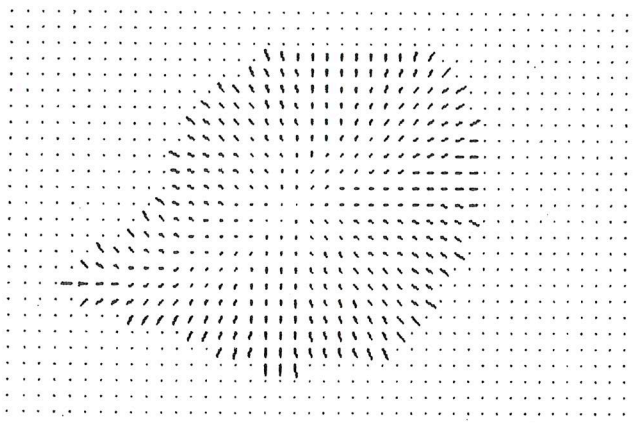

Figure 11-11. Needle diagram calculated by the iterative scheme under the assumption that the reflectance map is $\sec\theta_i$. (The surface orientation data are actually available on a finer grid; they are sampled coarsely here for display purposes.) The needle diagram is the estimate of the shape of the surface of the resin droplet shown in the previous figure. (Figure kindly provided by Katsushi Ikeuchi.)

The Euler equations in this case yield

$$\nabla^2 f = -\sum_{i=1}^{n} \lambda_i \big(E_i(x,y) - R_i(f,g)\big) \frac{\partial R_i}{\partial f},$$

$$\nabla^2 g = -\sum_{i=1}^{n} \lambda_i \big(E_i(x,y) - R_i(f,g)\big) \frac{\partial R_i}{\partial g}.$$

The corresponding discrete equations suggest an iterative scheme:

$$f_{kl}^{n+1} = \overline{f}_{kl}^{n} + \sum_{i=1}^{n} \lambda_i \big(E_{i;kl} - R_i(f_{kl}, g_{kl})\big) \frac{\partial R_i}{\partial f},$$

$$g_{kl}^{n+1} = \overline{g}_{kl}^{n} + \sum_{i=1}^{n} \lambda_i \big(E_{i;kl} - R_i(f_{kl}, g_{kl})\big) \frac{\partial R_i}{\partial g}.$$

The simple photometric stereo method discussed in the previous chapter can be used to obtain good initial values for $\{f_{kl}\}$ and $\{g_{kl}\}$. This will ensure rapid convergence to the solution.

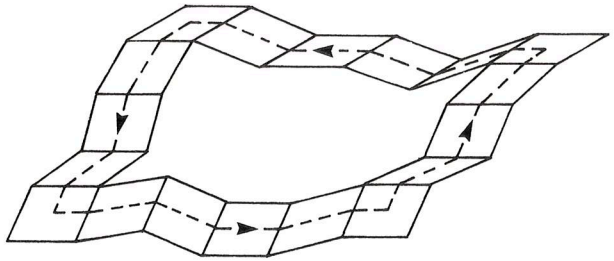

Figure 11-12. If surface orientation is known, elevation of the surface above some reference plane can be determined by integration along curves in the image. To be consistent, the integral of the surface gradient along a closed curve should be zero, since the overall change in elevation when one walks in a closed loop on a single-valued surface is zero.

11.8 Recovering Depth from a Needle Diagram

Several machine vision methods, including photometric stereo, produce surface shape information in the form of a *needle diagram*, in which surface orientation is given for every picture cell. In some cases we may want to represent surface shape in a different way. Often a *depth map*, giving height above some reference plane, is a desirable objective.

Given p and q, the partial derivatives of $z(x,y)$ with respect to x and y, we can recover $z(x,y)$ by integrating along arbitrary curves in the plane

$$z(x,y) = z(x_0,y_0) + \int_{(x_0,y_0)}^{(x,y)} (p\,dx + q\,dy).$$

In practice, p and q are recovered from noisy image data by imperfect methods. Thus the above integral might depend on the path chosen. Indeed, an integral along a closed path, as shown in figure 11-12, can be different from zero. Now since both p and q are available, we actually have more information than we really need. This suggests that we use a least-squares method to find the surface that best fits the imperfect estimate of the surface gradient.

We can, for example, choose $z(x,y)$ so as to minimize the error

$$\iint_I \big((z_x - p)^2 + (z_y - q)^2\big)\,dx\,dy,$$

where p and q are the given estimates of the components of the gradient, while z_x and z_y are the partial derivatives of the best-fit surface. Again, this is a problem in the calculus of variations. We have to minimize an

integral of the form

$$\iint F(z, z_x, z_y)\, dx\, dy.$$

The Euler equation is

$$F_z - \frac{\partial}{\partial x} F_{z_x} - \frac{\partial}{\partial y} F_{z_y} = 0,$$

so that from

$$F = (z_x - p)^2 + (z_y - q)^2$$

we obtain

$$\frac{\partial}{\partial x}(z_x - p) + \frac{\partial}{\partial y}(z_y - q) = 0,$$

or just

$$\nabla^2 z = p_x + q_y.$$

This equation accords with intuition, since it states that the Laplacian of the desired surface must equal $p_x + q_y$, which is an estimate of the Laplacian based on the given data.

As usual, we also need to know what to do about the boundary of the region over which this equation is to be solved. The *natural boundary condition* (see appendix) for an integral of the form

$$\iint F(z, z_x, z_y)\, dx\, dy$$

is

$$F_{z_x} \frac{dy}{ds} - F_{z_y} \frac{dx}{ds} = 0.$$

Here s is arclength along the boundary. We note at this point that $(dx/ds, dy/ds)^T$ is a tangent vector. In our case we obtain

$$(z_x - p)\frac{dy}{ds} = (z_y - q)\frac{dx}{ds},$$

or

$$(z_x, z_y)^T \cdot \left(\frac{dy}{ds}, -\frac{dx}{ds}\right)^T = (p, q)^T \cdot \left(\frac{dy}{ds}, -\frac{dx}{ds}\right)^T,$$

where the vector

$$\left(\frac{dy}{ds}, -\frac{dx}{ds}\right)^T$$

is a normal to the boundary curve at the point s. This result is eminently reasonable, since it states that the normal derivative of the desired surface must equal the estimate of the normal derivative obtained from the data.

An iterative method can be used to solve this equation. It can be based on a discrete approximation of the equation or a least-squares analysis applied directly to a discrete approximation of the original error integral, thus sidestepping the need for application of the calculus of variations.

Initial values can be generated by some simple scheme, such as integrating $p(x, 0)$ along the x-axis to obtain one profile, then integrating $q(x_0, y)$ along y starting at each point x_0 on the x-axis. (This crude method by itself, of course, does not produce a particularly good surface.)

11.9 References

The scanning electron microscope is described in *Scanning Electron Microscopy* by Wells [1974]. Many interesting pictures made using such instruments are shown in *Tissues and Organs: a Text-Atlas of Scanning Electron Microscopy* by Kessel & Kardon [1979] and in *Magnifications—Photography with the Scanning Electron Microscope* by Scharf [1977].

There are numerous books discussing partial differential equations, among them *Partial Differential Equations: Theory and Technique* by Carrier & Pearson [1976] and volume II of *Methods of Mathematical Physics* by Courant & Hilbert [1962]. But perhaps the most relevant for the first-order equations explored in this chapter is Garabedian's *Partial Differential Equations* [1964].

The calculus of variations is also the topic of many books, including *Calculus of Variations: With Applications to Physics & Engineering* by Weinstock [1974] and volume I of *Methods of Mathematical Physics* by Courant & Hilbert [1953]. In some of the exercises we relate the methods used in this chapter to *regularization* techniques for producing well-posed problems from ill-posed ones. Regularization is discussed by Tikhonov & Arsenin in *Solutions of Ill-Posed Problems* [1977].

There was a lot of interest in determining the shape of the surface features of the moon from telescopic images taken from the earth, at least until we could send probes, and finally people, to the vicinity of our rocky satellite. Since the libation of the moon, as well as the ratio of the radius of the earth to the distance between the two bodies, is small, we always see the moon from essentially the same direction. Thus binocular stereo can be ruled out as a viable method for recovering surface shape in this instance. Astronomers used shadows to estimate the relief of crater edges above the surrounding terrain. Van Digellen [1951] was the first to suggest the possibility of using shading, but he was only able to make some heuristic estimates of surface slope in the direction of the light source. Rindfleisch [1966] used photometric models developed in Russia by Fesenkov [1962] and others to derive a complex integration method for recovering the shape along profiles that we now know to be characteristic lines.

Horn [1970, 1975a] found the general solution of the shape-from-shading problem and later [1977] reworked the solution to make use of the reflectance map. Woodham [1979, 1981, 1984] provides excellent discussions of this topic, using the Hessian matrix as a tool.

The existence and uniqueness of solutions to the nonlinear first-order partial differential equation were explored by Bruss [1981, 1982, 1983], Brooks [1982], and Deift & Sylvester [1981].

Horn [1970] searched for a way to reformulate the problem so that the solution would take the form of a parallel iterative algorithm on a grid, much like the one he later used for the computation of lightness [1974]. Strat [1979] developed the first such algorithm. This algorithm was not, however, able to deal with the occluding boundary, since it used the gradient to parameterize surface orientation. Ikeuchi & Horn [1981] rectified this problem by introducing stereographic coordinates and a "lack-of-smoothness" term, now recognized as a regularization term. (For other ideas on parallel computation in vision, see Ballard, Hinton, & Sejnowshi [1983]. For a discussion of the use of regularization in dealing with ill-posed early vision problems, see Poggio & Torre [1984].)

Unfortunately the method of Ikeuchi and Horn, in turn, did not guarantee the integrability of the resulting needle diagram. Horn & Brooks [1985] have remedied this deficiency by using the surface normal to parameterize surface orientation. They avoid the use of a regularizing term in their work.

Shape can also be calculated from texture gradients or regular patterns; see Horn [1970], Bajcsy & Lieberman [1976], Witkin [1981], and Ikeuchi [1984]. These methods are inherently simpler, however, since more information is available at each image point than when shading is used.

Most shape-from-shading methods require that the reflectance map be given. There have been attempts to reduce dependence on such detailed knowledge. Pentland [1984], for example, tries to extract information locally. This inevitably requires strong assumptions, such as that the surface is spherical. Local methods cannot lead to unique results, since it is known from the work of Bruss [1981, 1982, 1983] and Brooks [1982] that singular points and occluding boundaries provide strong constraints, which are not available to a method that only considers shading in a small region of the image.

A compromise between exact knowledge of the reflectance map and not knowing anything at all is the use of a parameterized reflectance map. It is possible, for example, to recover the position of the light source from the image when certain assumptions are made. See Pentland [1982], Lee [1983], and Brooks & Horn [1985].

One can say something about the relationship between shading and surface shape without detailed solution of the image irradiance equation.

For an example, see Koenderink & van Doorn [1980]. The silhouette of the image of an object provides a great deal of information. Marr [1977] was concerned with the recovery of surface shape information from the occluding contour alone. Stevens [1981] considered the recovery of surface shape from special contours on the surface.

Much work has been devoted to understanding the interaction of light with the surface layer of an object. Typically a surface layer model is either so complex that only numerical results can be obtained or so simple as to be unrealistic. The photometric model of the lunar surface was refined by Minnaert [1961], whose reflectance function is used in exercise 11-1. Useful models for glossy reflection were developed by Torrance & Sparrow [1967] and Trowbridge & Reitz [1975].

11.10 Exercises

11-1 Consider a sphere of Lambertian material with center on the optical axis. Assume that the light source is a point source of unit intensity in the direction $(-p_s, -q_s, 1)^T$.

(a) What is the irradiance $E(x, y)$? Assume that the radius of the sphere is R and that the image is obtained using orthographic projection.

(b) Show that contours of constant brightness in the image are nested ellipses of equal eccentricity. Hint: What are the contours of constant brightness on the sphere?

(c) What do the contours of constant brightness in the image look like if we assume instead that the surface has the reflectance properties of the material in the maria of the moon? Hint: What are the contours of constant brightness on the sphere in this case?

11-2 Show that the slope of a surface in the direction that makes an angle θ with the x-axis is

$$m(\theta) = p\cos\theta + q\sin\theta.$$

Find the direction of steepest ascent. Conclude that the slope in the direction of steepest ascent is

$$m(\theta_s) = \sqrt{p^2 + q^2}.$$

11-3 Show that the two surfaces

$$z_1 = 2(x^2 + xy + y^2) \qquad \text{and} \qquad z_2 = (x^2 + 4xy + y^2)$$

give rise to the same shading near the origin if a rotationally symmetric reflectance map applies.